



Cite this: *Phys. Chem. Chem. Phys.*,
2017, 19, 6698

Super high-energy density single-bonded trigonal nitrogen allotrope—a chemical twin of the cubic *gauche* form of nitrogen†

Sergey V. Bondarchuk*^a and Boris F. Minaev^{ab}

A new ambient-pressure metastable single-bonded 3D nitrogen allotrope (TrigN) of trigonal symmetry (space group $R\bar{3}$) was calculated using density functional theory (DFT). A comprehensive characterization of this material, comprising thermodynamic, elastic, and spectral (vibrational, UV-vis absorption, and nuclear magnetic resonance) properties, was performed. Using high-throughput band structure calculation, the TrigN phase was characterized as an insulator with an indirect band gap of 2.977 eV. Phonon dispersion calculations justified that this structure is vibrationally stable at ambient pressure. The calculated Raman activities at the Γ -point demonstrated a rich pattern, whereas no relatively intense transitions were observed in its IR absorption spectrum. The TrigN material is almost transparent to visible light as well as to ultraviolet A and B. The main absorption peaks appeared within the range of 50–200 nm. The electron arrangement of the nitrogen nuclei in the studied nitrogen allotrope is much denser compared to that of the molecular nitrogen, which is in agreement with the calculated magnetic shielding tensor values. Robust mechanical stability is revealed from the elastic constants calculation. Due to strong anisotropy, the values of the Young's moduli vary from 281 to 786 GPa. A huge amount of internal energy is enclosed in the TrigN material. Upon decomposition to molecular nitrogen, the energy release is expected to be 11.01 kJ g⁻¹ compared to the value of 10.22 kJ g⁻¹ for the cubic *gauche* form of nitrogen. The TrigN allotrope possesses unique detonation characteristics with a detonation pressure of 146.06 GPa and velocity of 15.86 km s⁻¹.

Received 21st December 2016,
Accepted 31st January 2017

DOI: 10.1039/c6cp08723j

rsc.li/pccp

Introduction

Gaseous molecular nitrogen is the most abundant component of the Earth's atmosphere. It is one of the most stable molecules known because the dissociation energy of the triple N≡N bond is 954 kJ mol⁻¹. This is a reason why single-bonded nitrogen allotropes are so unusual and rare. Even molecular forms of nitrogen, other than N₂, have high energy densities,^{1,2} whereas infinite 1D, 2D, and 3D atomic frameworks form nitrogen phases possessing energy densities that are about five times higher than those of the most powerful non-nuclear weapons.³

However, to date, a number of different nitrogen allotropes have been predicted. The discovery of this phenomenon was first reported by McMahan *et al.*⁴ in 1985, and was then developed

in 1992.⁵ To date, several nitrogen phases have been reported and well-documented.^{6–17} The nitrogen allotropes that have been proposed are as follows: cubic *gauche* (cg-N),^{5–7} chaired web (CW),⁸ poly-N (pN),⁹ arsenic-like (A7),⁵ layered boat (LB),¹⁰ phosphorus-like (BP),⁵ metallic chain (CH),¹¹ zigzag chain (ZZ),¹² simple cubic (SC)¹³ allotropes, phases of the space groups *Pba2*,¹⁴ *P2₁2₁2₁*,¹⁴ *P1*,¹⁵ *C2/c*,¹⁵ *Cmcm*,¹⁵ and two molecular forms of N₂ (α -N₂ and ϵ -N₂),⁵ where the latter are based on the crystal structure determination of the former by Vegard.^{18,19}

However, Cui *et al.*¹⁶ concluded that in the pressure range from 0 to 360 GPa, the most favorable structures are *Cmcm*, A7, relative cubic *gauche* (rcg-N), cg-N, BP, *P2₁2₁2₁*, and *Pba2*. An interesting diamondoid (N₁₀-cage) nitrogen allotrope was recently proposed by Ma *et al.*¹⁷ This structure was found to be the most favored above 263 GPa. However, note that among the above-mentioned nitrogen allotropes, only the cg-N phase has been experimentally determined in 2004 by Eremets *et al.*^{20–22} by laser-heated diamond anvil cell experiments above 2000 K and 110 GPa. The phase is a robust material with a bulk modulus more than 300 GPa.²⁰ At ambient temperature, cg-N is metastable at pressures above 42 GPa and has unique properties including a high-energy density.^{6,20–22}

^a Department of Chemistry and Nanomaterials Science, Bogdan Khmel'nitsky Cherkasy National University, blvd. Shevchenko 81, 18031 Cherkasy, Ukraine.
E-mail: bondchem@cdu.edu.ua

^b Division of Theoretical Chemistry and Biology, School of Biotechnology, KTH Royal Institute of Technology, 10691 Stockholm, Sweden

† Electronic supplementary information (ESI) available: Crystal packing, graphical description of the vibrational modes, optical and thermodynamic properties, and also elastic stiffness and compliance constants. See DOI: 10.1039/c6cp08723j

To search for novel high-energy density materials (HEDM), calculations of different isolated molecular forms of nitrogen were performed.^{3,23–47} As a result, a number of different neutral and ionic species were subsequently modeled theoretically and/or detected experimentally. The vibrationally stable structures include N_3^- ,^{3,23} N_4 ,^{24–28} N_5^- ,^{29–31} N_5^+ ,^{30,32,33} N_6 ,^{26,27,34–41} N_8 ,^{27,42–44} N_{10} ,^{45,46} and N_{60} ^{45,47} species. Moreover, the systems with N_4 and N_5 stoichiometry have been well reviewed.³² To the best of our knowledge, only three ionic structures have been experimentally observed among the abovementioned nitrogen forms.³ The well-known azide anion (N_3^-) has moderate stability, whereas the pentanitrogen cation (N_5^+) is metastable and can exist only with large counter anions. Moreover, the pentanitrogen anion (N_5^-) has been detected only in the gas phase.³

The aim of the present study was to search for potentially favorable nitrogen phases that demonstrate high-energy density, dynamical stability at low pressure, and robust mechanical characteristics that are comparable or better than that of the experimentally obtained cg-N phase.²⁰ The reported results suggest that the simulated TrigN allotrope conforms to all the abovementioned conditions. Therefore, if synthesized, this structure will be a potentially favorable, green high explosive possessing enhanced detonation properties.

Computational details

The first principles calculations of the equilibrium geometries, spectral, thermodynamic, and mechanical properties presented in this study were performed using the Cambridge Serial Total Energy Package (CASTEP) module⁴⁸ implemented in the Materials Studio 7.0 program suite⁴⁹ within the generalized gradient approximation (GGA). Exchange and correlation interactions were described using the functional parameterized by Perdew–Burke–Ernzerhof (PBE),⁵⁰ except for the mechanical properties calculations for which the interactions were described using the PBE for solids (PBESol) functional.⁵¹ Moreover, for band structure calculations, we used a more accurate hybrid exchange–correlation functional by Heyd–Scuseria–Ernzerhof (HSE06).⁵² A norm-conserving pseudopotential (NCP) in reciprocal space was entirely used to describe the electron-core interactions. In the case of the equation of state calculations, the projector augmented wave based method (PAW)⁵³ was used instead of the previous approach. These calculations were performed using the Quantum Espresso 4.3.2 suite of programs.⁵⁴ For all the calculations, the electronic wave functions were expanded in a plane wave basis set with an energy cut-off of 1000 eV (73.5 Ry). The Monkhorst–Pack k -point sampling scheme with a $8 \times 8 \times 8$ (0.03 \AA^{-1}) k -point mesh was specified during all the calculations. The SCF tolerance was set to be equal 1×10^{-6} eV per atom and the force convergence criterion during the optimizations was set to be 1×10^{-2} eV \AA^{-1} .

For the GGA/PBE approach, the long-range electron correlations entirely were considered during the calculation using the Tkatchenko–Scheffler (TS) scheme,⁵⁵ which has been proven to

produce reliable results.⁵⁶ Therefore, the C_6 coefficients were calculated using the following equation:

$$C_{6AA}^{\text{eff}} = \frac{\eta_A^{\text{eff}}}{\eta_A^{\text{free}}} \left(\frac{\kappa_A^{\text{free}}}{\kappa_A^{\text{eff}}} \right)^2 \left(\frac{V_A^{\text{eff}}}{V_A^{\text{free}}} \right)^2 C_{6AA}^{\text{free}}, \quad (1)$$

where η is the effective frequency, V is the atomic volume, and κ is the proportionality constant between volume and polarizability for the free atom and the atom in a molecule. Superscripts “free” and “eff” stand for the isolated atom and the atom in a molecule, respectively. The phase decomposition energy was calculated according to eqn (2) and the cohesive energy was obtained using eqn (3):

$$E_{\text{dec}} = E_{\text{TrigN}} - 6E_{N_2} \quad (2)$$

$$E_{\text{coh}} = -(E_{\text{TrigN}} - 12E_N)/12 \quad (3)$$

where E_{TrigN} is the total energy (PBE-TS) of the TrigN unit cell, and E_{N_2} and E_N are the total energies of an isolated nitrogen molecule and atom, respectively. The latter were obtained using the supercell approximation (vacuum slab thickness is 15 Å). The phonon dispersion calculation was carried out in terms of the finite displacement method. The latter provides reliable results even when ultrasoft pseudopotentials are used.⁵⁷ Molecular visualizations were performed using the Virtual NanoLab 2015.1 program package.⁵⁸

Results and discussion

Structural features and electronic properties

Geometry optimization with complete cell relaxation led to a trigonal nitrogen allotrope of the space group $R\bar{3}$. This space group can be presented in two ways using the rhombohedral-centered hexagonal (HEX) or primitive-centered rhombohedral (RHL₂) (for $\alpha > 90^\circ$) lattice. The latter representation corresponds to the primitive cell for the trigonal crystal system of the Laue class $\bar{3}$. The nitrogen atoms occupy the Wyckoff positions 18f: N1 (0.245, 0.957, and 0.863) and N2 (0.245, 0.957, and 0.363) in the hexagonal lattice as well as N1 (0.925, 0.594, and 0.393) and N2 (0.893, 0.425, and 0.094) in the rhombohedral lattice. The corresponding unit cell projections are illustrated in Fig. 1 and the optimized asymmetric cell parameters are listed in Table 1.

As can be seen in Fig. 1, the HEX unit cell contains 36 nitrogen atoms and the RHL₂ cell includes 12 atoms. The latter space group representation is much more convenient for the analysis and is directly related to the corresponding hexagonal lattice. The use of both lattices produces very close values of the calculated properties; therefore, the RHL₂ cell has been discussed hereinafter since this is the simplest representation of the space group $R\bar{3}$, which still cannot be reduced by symmetry. All the N–N bonds inside the cell are symmetrically equivalent with the length being equal to 1.436 Å, which is very close to the cg-N allotrope (1.434 Å). However, the experimentally measured N–N bond lengths in the cg-N phase are 1.346 Å.²⁰ Therefore, we speculate that these bonds should be similar to those of the

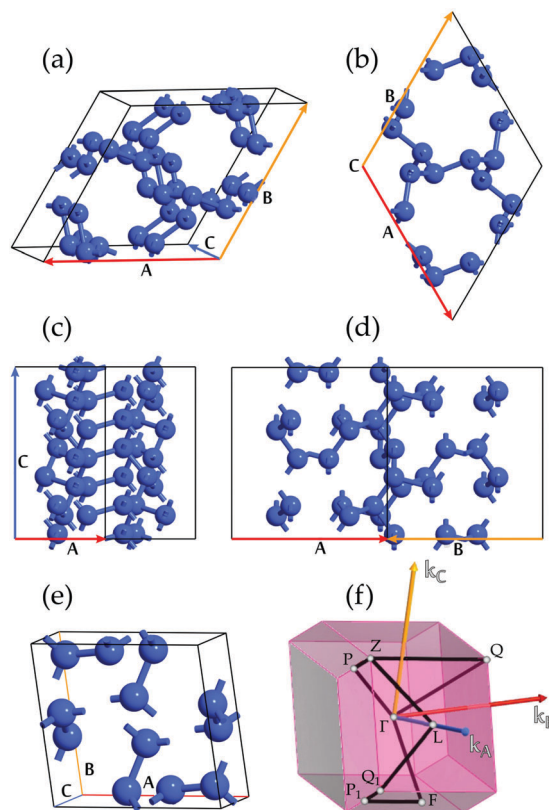


Fig. 1 Projections of the unit cell in the hexagonal representation (a–d) and in the RHL₂ representation (e), and the Brillouin zone with the corresponding high symmetry points for the latter case (f).

Table 1 The optimized asymmetric cell parameters of the TrigN allotrope in hexagonal (HEX) and rhombohedral (RHL₂) representations

Lattice	a (Å)	c (Å)	Lattice	a (Å)	α (°)
HEX	6.886	6.630	RHL ₂	4.548	98.39

TrigN allotrope. The crystal packing of the TrigN phase is illustrated in Fig. S1 in the ESI.†

At zero external pressure, the cell volume is equal to 89.74 Å³. Therefore, the calculated crystal density equals 3.11 g cm⁻³. To elucidate the effect of external pressure, we calculated the enthalpies and volumes of the TrigN and cg-N allotropes together with α -N as a reference and the results are illustrated in Fig. 2a and b.

These calculations confirm that the cg-N phase becomes more preferable than α -N above 53 GPa, and TrigN behaves similarly since it is more stable than α -N above 66 GPa (Fig. 2a). However, note that the cg-N allotrope is always lower in energy than TrigN by about 0.17–0.20 eV. Very similar behavior of the TrigN and cg-N allotropes can be clearly observed from the pressure-dependence of the cell volume (Fig. 2b). We also performed the equation of state $E(V)$ calculations (Fig. 2c). The E vs. V data were fitted by the third-order Birch–Murnaghan (BM) equation of state. The fitted parameters are listed in Table 2. The equilibrium volumes are close for the cg-N and TrigN allotropes, whereas the bulk modulus is lower than that for the latter phase.

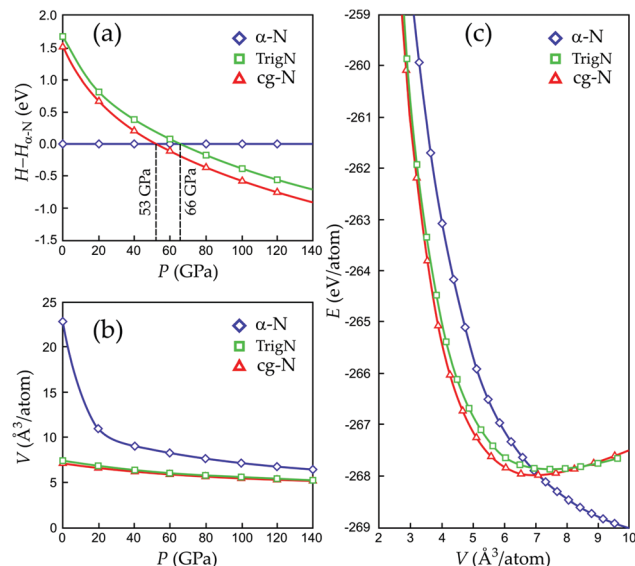


Fig. 2 Pressure-dependence of the relative enthalpies (a) and volume (b), and the equation of state $E(V)$ (c).

Table 2 The results of the third-order BM equation of state fitting

Phase	E_0	V_0	B_0	B_0'
α -N	-269.57	22.82	7.2	4.05
cg-N	-267.91	7.08	189.8	5.10
TrigN	-267.80	7.46	142.2	5.96

To study the electronic properties of the TrigN allotrope, we performed band structure calculations. To find the most appropriate approximation combining high rigor and low-computational cost, we examined both the effect of the k -point sampling mesh and basis set energy cut-off on the band gap values. The band structure calculations were performed in terms of the high-throughput approach, which includes a standard definition of the high symmetry k -path for all the 14 Bravais lattices.⁵⁹ In the case of the rhombohedral RHL₂ lattice, the coordinates of the high symmetry points are presented in Table 3 and the Brillouin zone path is illustrated in Fig. 1f. The band structure plot obtained using the NCP/HSE06/700 eV approach is illustrated in Fig. 3. In Table 3, $\eta = 1/(2 \tan^2(\alpha/2))$ and $\nu = 3/4 - \eta/2$.⁵⁹

As can be seen in Fig. 3, the TrigN allotrope possesses an indirect band gap since the valence band maximum (VBM) and conduction band minimum (CBM) lie at different k -vectors. Note that the gap width is strongly dependent on the method applied. Therefore, the correct description of the gap width is a challenging task. If the accuracy of the used approximation is

Table 3 Definition of high symmetry k -points in the RHL₂ ($\alpha > 90^\circ$) case of rhombohedral lattice

k	$\times k_A$	$\times k_B$	$\times k_C$	k	$\times k_A$	$\times k_B$	$\times k_C$
Γ	0	0	0	P_1	ν	$\nu - 1$	$\nu - 1$
F	1/2	-1/2	0	Q	η	η	η
L	1/2	0	0	Q_1	$1 - \eta$	$-\eta$	$-\eta$
P	$1 - \nu$	$-\nu$	$1 - \nu$	Z	1/2	-1/2	1/2

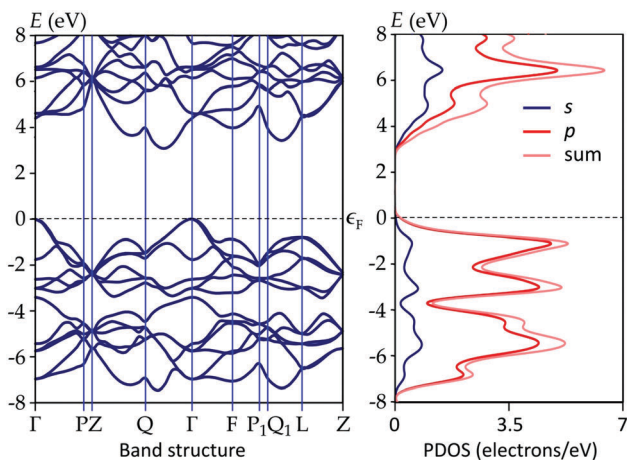


Fig. 3 Band structure and partial density of states (PDOS) for the TrigN allotrope calculated using the NCP/HSE06/700 eV approach.

appropriate for the calculation, the band gap width is only related to the method applied to describe the exchange–correlation term. However, in the case of an inappropriate Brillouin zone integration, one can provide a wrong conclusion about the nature of the band gap.⁵⁹ For this purpose, we used a standardized scheme, the high-throughput approach, for Brillouin zone integration.⁵⁹ Moreover, while using hybrid functionals for band structure calculations, which require a huge computational cost, a set of minimum accuracy parameters needs to be determined. These include (i) density of the k -points, (ii) cut-off energy, and (iii) computational approach (potential/functional). Therefore, we attempted to account for the influence of the latter three factors within the following set of trials.

Preliminary band structure calculations using the NCP/PBE-TS/1000 eV approach provide a gap value that is equal to 1.517 eV. However, it has been recently found that the hybrid functional HSE06 usually provides gaps closer to the experimental values than the GGA functionals.⁶⁰ However, considering that HSE06 requires a huge computational cost, we performed a set of calculations for the band gap with the NCP/PBE-TS approach using different cut-off energies (from 100 to 1000 eV) and different k -point sampling $n \times n \times n$ (n changes from 1 to 8). The abovementioned functional was chosen because of its computational ease. The results are graphically shown in Fig. S2 and the tabulated data are presented in Table S1 in the ESI.†

As can be seen in Fig. S2 (ESI†), the band gap values strongly increase towards higher cut-off energies. When small cut-off energies (100–200 eV) are used, the values obtained are negative. In addition, more or less reproducible results appear when a cut-off energy of 700 eV is applied. The influence of k -point sampling is less pronounced. Even when only the Γ -point is applied, the band gap is about 80–90% from the value obtained using the densest grid. Generally, the mesh of $4 \times 4 \times 4$ is enough to obtain a stable result (Fig. S2, ESI†). Therefore, the calculation at the NCP/HSE06/700 eV level of theory and a $4 \times 4 \times 4$ grid provided the band gap values equals to 2.977 eV and 2.962 eV in the HEX lattice case (Fig. 3). To check if the HSE06 results exhibit the same trend as that of the PBE-TS functional, we performed one

more calculation using 500 eV with a $3 \times 3 \times 3$ mesh. In this case, the band gap was 2.923 eV, thus proving that the HSE06 results show the same trend as those for the PBE-TS functional (Table S1, ESI†). The obtained value is much lower than that of cg-N phase, which was found to be 8.1 eV using the Monte Carlo method.⁶¹

Spectral pattern and phase stability

To ensure that the predicted TrigN nitrogen allotrope is dynamically stable, we performed phonon dispersion calculations. Remarkably, this structure displays no soft modes even at zero external pressure. The high-symmetry points within the Brillouin zone were chosen in accordance with the abovementioned high-throughput approximation.⁵⁹ The obtained plot along with the calculated phonon density of states is illustrated in Fig. 4. Since the RHL₂ lattice of the TrigN phase contains 12 nitrogen atoms, this results in a total of 36 phonon branches. As can be seen in Fig. 4, the acoustic branches remain linear in the region of the small k -points. Moreover, towards the Γ –Q direction, two modes are degenerate, which suggests the equality of the sound velocity values. Upon applying an external pressure, the TrigN allotrope conserves dynamical stability at least up to 200 GPa.

We also performed infrared (IR) intensities and Raman activities calculation at the Γ -point. These data together with the corresponding vibrational frequencies are listed in Table 4. The symmetry constraints lead to 11 doubly-degenerate modes with a total of 33. Moreover, similar to the vibrational spectra of the 2D nitrogen phases of the A7 and zigzag sheet (ZS) topologies,⁶² the IR spectrum of TrigN also does not provide much information because most of the vibrations are strongly forbidden by symmetry. However, the Raman spectrum is much more informative (Table 4). Above 459 cm^{-1} , the TrigN phase becomes visible for Raman spectroscopy. Especially, the vibration of the a_g symmetry at 873.88 cm^{-1} , which has Raman activity equal to 4632.9 \AA^4 (Table 4). The form of vibrations can be found in Fig. S3 in the ESI.†

Spectral identification of the TrigN phase can also be performed *via* UV-vis spectroscopy. To obtain the corresponding

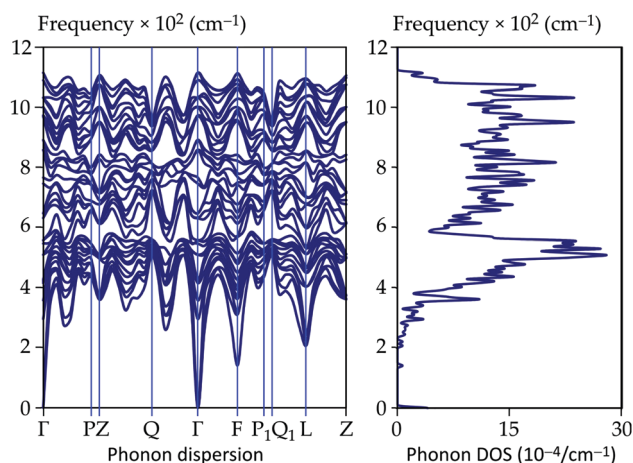


Fig. 4 Phonon dispersion and density of phonon states for the TrigN allotrope.

Table 4 The calculated IR and Raman spectra of the TrigN allotrope

Mode	Symmetry	ν (cm ⁻¹)	IR (km mol ⁻¹)	Raman (Å ⁴)
1	e _u	285.24		
2	e _u	285.24		
3	a _u	379.34		
4	a _u	423.78	0.2939	
5	a _u	437.11		
6	e _g	459.07		260.3247
7	e _g	459.07		260.7697
8	e _g	481.89		0.4740
9	e _g	481.89		1.4186
10	a _g	542.38		0.2945
11	a _g	545.02		394.2054
12	e _u	597.55	1.0502	
13	e _u	597.55	1.0502	
14	e _u	623.85		
15	e _u	623.85		
16	a _g	696.18		0.6057
17	a _g	718.38		668.5242
18	e _g	798.68		642.6735
19	e _g	798.68		643.3702
20	e _g	855.79		0.5255
21	e _g	855.79		1.5744
22	a _g	873.88		4632.8956
23	a _u	874.10		
24	e _u	875.17		
25	e _u	875.17		
26	a _u	886.83	3.2558	
27	e _u	898.82	2.8881	
28	e _u	898.82	2.8881	
29	e _g	933.46		0.3398
30	e _g	933.46		0.9983
31	a _g	948.34		0.2858
32	e _g	1006.89		181.5198
33	e _g	1006.89		182.1329

optical properties, we carried out the calculations of the complex dielectric function $\varepsilon(\omega) = \varepsilon_1(\omega) + i\varepsilon_2(\omega)$. Herein, the imaginary part includes momentum matrix elements, which allow the description of the electronic transition between the valence and conducting bands in a solid (eqn (4)).⁶²

$$\varepsilon_2(\omega) = \frac{1}{4\pi\varepsilon_0} \left(\frac{2\pi e}{m\omega} \right)^2 \sum_{\mathbf{k}, \mathbf{c}, \mathbf{v}} |\langle \psi_{\mathbf{k}}^{\mathbf{c}} | e\mathbf{p} | \psi_{\mathbf{k}}^{\mathbf{v}} \rangle|^2 \delta(E_{\mathbf{k}}^{\mathbf{c}} - E_{\mathbf{k}}^{\mathbf{v}} - \hbar\omega), \quad (4)$$

where subscripts c and v indicate conducting and valence band states, respectively. The imaginary part of the function was also used to obtain the real part $\varepsilon_1(\omega)$ in terms of the Kramer–Kronig transform (eqn (5)).⁶³

$$\varepsilon_1(\omega) = 1 + \left(\frac{2}{\pi} \right) \int_0^{\infty} d\omega' \frac{\omega'^2 \varepsilon_2(\omega')^2}{\omega'^2 - \omega^2} \quad (5)$$

Therefore, the absorption coefficient (α) can be expressed as follows (eqn (6)):

$$\alpha(\omega) = \sqrt{2} \left[\sqrt{\varepsilon_1^2(\omega) + \varepsilon_2^2(\omega)} - \varepsilon_1(\omega) \right]^{1/2} \quad (6)$$

The calculated absorption spectrum of the TrigN allotrope is presented in Fig. 5. The dielectric function itself and the other derivative optical properties, such as reflectivity, refractive index, conductivity, and loss function, are illustrated in Fig. S4 in the ESI.† Due to the symmetry constraints, the absorption spectra

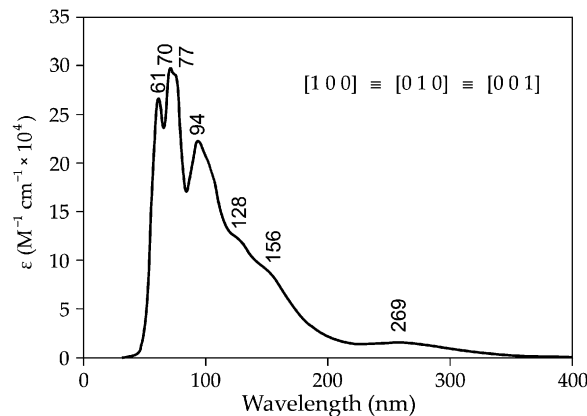


Fig. 5 Calculated absorption spectrum of the TrigN allotrope.

calculated for the three directions of the polarized incident light ([1 0 0] ≡ [0 1 0] ≡ [0 0 1]) are identical. The optical properties were calculated at the NCP/HSE06/700 eV level of theory, which is sufficient for this case.⁶⁰ As can be seen in Fig. 5, the lowest-energy band has a λ_{max} of 269 nm. Note that we detected the positions of λ_{max} using the plot of $\partial^2\varepsilon/\partial E^2$ vs. E . Therefore, the abovementioned band does not correspond to the VBM–CBM transition, which is significantly red-shifted.

According to the band structure plot, the lowest-energy band corresponds to the Γ – Γ electronic transition. The remaining higher-energy bands include electron transitions from the deeper valence bands (Fig. 3). Therefore, the TrigN allotrope is transparent to visible light as well as to the ultraviolet A and B regions. The strongest absorption corresponds to the vacuum ultraviolet in the range from 60 to 100 nm (Fig. 5).

To gain additional information on the spectral identification and bonding of the TrigN allotrope, we calculated its nuclear magnetic resonance (NMR) properties using the gauge-including projector augmented-wave method (GIPAW)⁶⁴ and electric field gradient (EFG) at the nuclei. Nitrogen possesses two NMR-active isotopes: ¹⁴N ($I = 1$) and ¹⁵N ($I = 1/2$). Despite the fact that ¹⁴N has a very high natural abundance (99.63%), it is rarely used in solid-state NMR spectroscopy.^{65,66} The obtained data are listed in Table 5. We compared these results with those previously calculated for the A7 and ZS nitrogen sheets⁶² and the bare nitrogen molecule. Since the choice of NMR reference in theoretical calculations may become crucial,⁶⁷ we analyzed only the absolute values of the shielding tensors.

Table 5 Chemical shielding and electric field gradient (EFG) tensors at the symmetry unique atoms in the TrigN allotrope

Atom	Shielding tensor			EFG tensor	
	σ_{iso}^a (ppm)	Δ^b (ppm)	η^c	C_Q^d (MHz)	η_Q^e
N1	−29.74	−35.92	0.53	−7.80	0.07
N2	−29.75	−35.93	0.52	−7.80	0.07

^a $\sigma_{\text{iso}} = (\sigma_{xx} + \sigma_{yy} + \sigma_{zz})/3$. ^b $\Delta = \sigma_{zz} - \sigma_{\text{iso}}$. ^c $\eta = (\sigma_{xx} - \sigma_{yy})/\Delta$. ^d $C_Q = eQV_{zz}/h$, where V_{zz} is the largest component of the diagonalized EFG tensor, Q is the nuclear quadrupole moment, and h is the Planck's constant. ^e $\eta_Q = (V_{xx} - V_{yy})/V_{zz}$.

As can be seen in Table 5, the σ_{iso} values for the symmetry unique nitrogen atoms in the TrigN allotrope are much higher than those for the A7 and ZS polynitrogen sheets, which vary from -62.51 to -64.51 ppm.⁶² These are higher than the values of the σ_{iso} for molecular nitrogen (-91.33 ppm), which is in agreement with our calculations, and are shifted towards a stronger field. Therefore, TrigN has a denser electron arrangement compared to molecular nitrogen. Among the EFG derived parameters, we estimated the quadrupolar coupling constants (C_Q) and quadrupolar asymmetry parameter (η_Q) (Table 5). The negative values of the C_Q constants suggest that the nuclei have an oblate spheroid shape along the spin axis. In the case of the TrigN phase, this effect is more pronounced than in the molecular nitrogen (-5.60 MHz).⁶²

Mechanical properties

To estimate the mechanical robustness of the TrigN allotrope, we calculated the corresponding elastic constants. The values of the elastic stiffness (C_{ij}) and compliance (S_{ij}) constants are listed in Tables S2 and S3 in the ESI† To be mechanically stable, the independent elastic constants of a crystal should satisfy the corresponding Born–Huang criteria. The rhombohedral lattice of the Laue class $\bar{3}$ possesses 7 independent elastic constants and, subsequently, 4 necessary and sufficient criteria.⁶⁸

$$\begin{cases} C_{11} > |C_{12}|; & C_{44} > 0; \\ C_{13}^2 < 1/2C_{33}(C_{11} + C_{12}); \\ C_{14}^2 + C_{15}^2 < 1/2C_{44}(C_{11} - C_{12}) \equiv C_{44}C_{66}. \end{cases} \quad (7)$$

As can be seen in Table S2 (ESI†), the TrigN allotrope elasticity obeys the criteria shown in eqn (7). Moreover, we constructed 3D contours of the Young's modulus on the basis of the elastic compliance constants (S_{ij}) according to eqn (8).⁶⁹

$$\frac{1}{E} = (1 - l_3^2)^2 s_{11} + l_3^4 s_{33} + l_3^2 (1 - l_3^2) (2s_{13} + s_{44}) + 2l_2 l_3 (3l_1^2 - l_2^2) s_{14} + 2l_1 l_3 (3l_2^2 - l_1^2) s_{25} \quad (8)$$

where $l_1 = \sin \theta \cos \varphi$, $l_2 = \sin \theta \sin \varphi$, and $l_3 = \cos \theta$ are the directional sines and cosines of angles with the three principal directions. The obtained 3D plots together with the projections on the secant planes are illustrated in Fig. 6 and the results of the direct calculations of the elastic properties are summarized in Table 6.

The TrigN allotrope exhibits strong anisotropy of the Young's modulus. Along the z axis, the E value is rather high and equals 785.7 GPa, which is about two-third to that of diamond (1050–1210 GPa), which is the hardest material known.⁷⁰ In contrast, along the x and y directions, the Young's moduli are much lower. The bulk modulus is equal to 192.5 GPa, which follows from the direct calculation using the NCP/PBESol/1000 eV approach. The value obtained by fitting the MB equation (PAW/PBE/1000 eV method) is equal to 142.2 GPa. Note that the previously obtained value of the bulk modulus of the cg-N allotrope equals 298–301 GPa by fitting different equations of state.²⁰ We recalculated the latter quantity using the direct

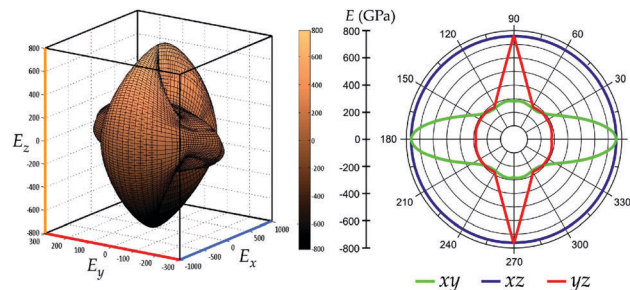


Fig. 6 3D plot of the Young's modulus of the TrigN allotrope together with the three projections on the secant planes.

Table 6 Young's modulus (E , GPa) and Poisson ratios (ν) for the TrigN allotrope

Axis	E (GPa)	Poisson ratios (ν)			
x	280.6201	E_{xy}	0.2789	E_{xz}	0.0853
y	280.6201	E_{yx}	0.2789	E_{yz}	0.0853
z	785.7471	E_{zx}	0.2389	E_{zy}	0.2389

NCP/PBESol/1000 eV approach and obtained a bulk modulus equal to 273 GPa. Therefore, we can conclude that the TrigN allotrope is a slightly less robust solid compared to the cg-N phase.

Thermodynamics and energy density

Based on the phonon calculations, we estimated the thermodynamic properties of the TrigN allotrope in the temperature range from 0 to 1000 K. These include zero-point vibrational energy (ZPE), enthalpy (H), entropy (S), Gibbs free energy (G), constant volume heat capacity (C_v), and the Debye temperature (Θ_D), which can be expressed as follows:

$$\Theta_D = \frac{h}{k_B} \sqrt[3]{\frac{3n}{4\pi} \left(\frac{N_A \rho}{M} \right) \nu_m} \quad (9)$$

where h is the Planck constant, k_B is the Boltzmann constant, n is the number of atoms per unit cell, N is the Avogadro number, ρ is the crystal density, M is the molecular weight, and ν_m is the average sound velocity. The results are graphically presented in Fig. S5 in the ESI† and the numerical values at 298 K along with the other parameters are listed in Table 7.

The cohesive energy of the studied allotrope is 6.52 eV, whereas that of the cg-N phase has a value equal to 6.63 eV. These two materials have huge robustness of the solid state compared to α -N, which has a value of 0.080 eV, in accordance with the calculations presented herein. Despite the recently predicted molecular forms of nitrogen, N_6 and N_8 are more thermodynamically favored than the TrigN and cg-N allotropes since these have the cohesive energies that are about only 4–5 times stronger than those in solid N_2 . Thus, the cohesive energies are 0.307 eV (N_6)¹ and 0.426 eV (N_8)².

Although an energy density value of 27.89 kJ g^{-1} was reported for the cg-N phase,⁷¹ a lack of calculation details is a reason why we could not reproduce this energy density value during the present study. Moreover, at the GGA/PBE level of theory, the calculated

Table 7 The calculated thermodynamic properties (at 298 K) for the TrigN nitrogen allotrope

ZPE ^{a,b}	H ^b	G ^b	TS ^b	C _V ^c	Θ _D ^d	Θ _D ^{lim e}
137.32	12.81	-5.25	18.06	29.13	1301	1914

^a Zero point energy. ^b Values in kJ mol⁻¹. ^c Value in cal cell⁻¹ K⁻¹.
^d Value obtained at 131 K. ^e Value corresponds to the high temperature limit (K).

energy density was found to be 9.7 kJ g⁻¹.⁷² This value is very close to that obtained in the present study (10.22 kJ g⁻¹). Probably, this big difference between the calculated values of energy density of the cg-N allotrope is related to the calculation methods applied. As is known that the absolute values of the calculated energies significantly depend on the calculation method applied, therefore, we computed and compared the energy density values for the TrigN and cg-N allotropes to obtain a relative description. The energy density value for the TrigN allotrope equals 11.01 kJ g⁻¹, which is slightly higher than that of cg-N. The abovementioned molecular forms (N₆ and N₈) are characterized by much lower values equal to 2.30 and 2.43 kJ g⁻¹, respectively.^{1,2}

Upon decomposition to molecular nitrogen, the TrigN allotrope releases 1850.76 kJ mol⁻¹ and the relative increase in the volume is V₂/V₁ = 2487. Taking the value of 1850.76 kJ mol⁻¹ as the enthalpy of formation of the TrigN phase, we applied the Kamlet–Jacobs empirical scheme to determine three important detonation parameters such as detonation energy (*Q*, cal g⁻¹), pressure (*P*, GPa), and velocity (*D*, km s⁻¹).⁷³ Although this method was developed for C–H–N–O explosives, it can be effectively applied to nitrogen allotropes that are expected to be metastable at zero external pressure and decompose to molecular nitrogen. Thus, the detonation pressure and velocity can be calculated according to eqn (10) and (11).⁷³

$$D = 1.01(N\bar{M}^{1/2}Q^{1/2})^{1/2}(1 + 1.30\rho_0) \quad (10)$$

$$P = 1.558\rho_0^2 N\bar{M}^{1/2}Q^{1/2} \quad (11)$$

where *N* and \bar{M} are dimensionless structure-derived quantities. These two parameters along with the *Q* value can be calculated in three ways depending on the appropriate structure criterion in which the studied system falls. Since the TrigN does not include any oxidants and reductants, the appropriate structural criterion is as follows: $d \geq 2a + b/2$, where *a*, *b*, and *d* stand for the number of carbon, hydrogen, and oxygen atoms in the asymmetric cell, respectively. Therefore, the *N*, \bar{M} , and *Q* quantities were calculated as follows (eqn (12) and (13)):⁷³

$$N = \frac{1}{M} = \frac{2c}{4MW} \quad (12)$$

$$Q = \frac{239\Delta H_f^0}{MW} \quad (13)$$

where *c* stands for the number of nitrogen atoms per asymmetric cell and MW is the molecular weight.

According to our results, the calculated *Q*, *P*, and *D* parameters for the TrigN phase are 2631.66 cal g⁻¹, 146.06 GPa,

and 15.86 km s⁻¹, respectively. These enhanced detonation parameters are a few times higher than those of the most powerful examples of conventional explosives. For these explosives, the range of detonation pressure is about 20–40 GPa and the detonation velocity is about 7–10 km s⁻¹.^{74–76}

Conclusions

In summary, we predicted and described a novel nitrogen allotrope of the trigonal crystal system and rhombohedral lattice type, which is called TrigN. This new phase can be characterized as a chemical twin for the experimentally obtained cg-N allotrope. Almost all the studied physical properties of these two structures are rather similar, whereas the mechanical stability of the cg-N phase is slightly better. Moreover, the energy density of the TrigN phase is higher, which implies a more enhanced detonation performance.

In addition, note that the recent interest for molecular crystal forms of nitrogen,^{1,2} as well as for molecules including nitrogen–boron strained cycles, is increasing.⁷⁴ 2D materials with similar structural motifs have been recently reported.⁷⁷ Indeed, the molecular forms are expected to be much more stable than the solid forms of nitrogen, such as TrigN or cg-N. The latter forms can scarcely be simply applied as explosives because these forms suffer from a lack of stability. Therefore, the computational search for potentially preferable high-energy density new molecular crystal forms of nitrogen represents definite importance due to high environmental safety and unique detonation characteristics.

Acknowledgements

This work was supported by the Ministry of Education and Science of Ukraine, Research Fund (Grant No. 0113U001694). We thank Professor Hans Ågren (KTH, Stockholm) for the PDC supercomputer use. The computations were performed *via* the resources provided by the Swedish National Infrastructure for Computing (SNIC) at the Parallel Computer Center (PDC) through the project “Multiphysics Modeling of Molecular Materials”, SNIC 020/11-23.

Notes and references

- M. J. Greschner, M. Zhang, A. Majumdar, H. Liu, F. Peng, J. S. Tse and Y. Yao, *J. Phys. Chem. A*, 2016, **120**, 2920.
- B. Hirshberg, R. Benny Gerber and A. I. Krylov, *Nat. Chem.*, 2014, **6**, 52.
- T. M. Klapötke, *New Nitrogen-Rich High Explosives*, in *High Energy Density Materials*, ed. T. M. Klapötke, Springer-Verlag GmbH, Berlin, 2007, vol. 125, pp. 85–121.
- A. K. McMahan and R. LeSar, *Phys. Rev. Lett.*, 1985, **54**, 1929.
- C. Mailhot, L. H. Yang and A. K. McMahan, *Phys. Rev. B: Condens. Matter Mater. Phys.*, 1992, **46**, 14419.
- M. I. Eremets, A. G. Gavriliuk, N. R. Serebryanaya, I. A. Trojan, D. A. Dzivenko, R. Boehler, H. K. Mao and R. J. Hemley, *J. Chem. Phys.*, 2004, **121**, 11296.

- 7 X.-Q. Chen, C. L. Fu and R. Podloucky, *Phys. Rev. B: Condens. Matter Mater. Phys.*, 2008, **77**, 064103.
- 8 F. Zahariev, J. Hooper, S. Alavi, F. Zhang and T. K. Woo, *Phys. Rev. B: Condens. Matter Mater. Phys.*, 2007, **75**, 140101(R).
- 9 A. R. Oganov and C. W. Glass, *J. Chem. Phys.*, 2006, **124**, 244704.
- 10 F. Zahariev, A. Hu, J. Hooper, F. Zhang and T. Woo, *Phys. Rev. B: Condens. Matter Mater. Phys.*, 2005, **72**, 214108.
- 11 M. M. G. Alemany and J. Luis Martins, *Phys. Rev. B: Condens. Matter Mater. Phys.*, 2003, **68**, 024110.
- 12 W. D. Mattson, D. Sanchez-Portal, S. Chiesa and R. M. Martin, *Phys. Rev. Lett.*, 2004, **93**, 125501.
- 13 J. Kotakoski and K. Albe, *Phys. Rev. B: Condens. Matter Mater. Phys.*, 2008, **77**, 144109.
- 14 Y. Ma, A. R. Oganov, Z. Li, Y. Xie and J. Kotakoski, *Phys. Rev. Lett.*, 2009, **102**, 065501.
- 15 Y. Yao, J. S. Tse and K. Tanaka, *Phys. Rev. B: Condens. Matter Mater. Phys.*, 2008, **77**, 052103.
- 16 X. Wang, F. Tian, L. Wang, T. Cui, B. Liu and G. Zou, *J. Chem. Phys.*, 2010, **132**, 024502.
- 17 X. Wang, Y. Wang, M. Miao, X. Zhong, J. Lv, T. Cui, J. Li, L. Chen, C. J. Pickard and Y. Ma, *Phys. Rev. Lett.*, 2012, **109**, 175502.
- 18 L. Vegard, *Nature*, 1929, **124**, 267.
- 19 L. Vegard, *Nature*, 1929, **124**, 337.
- 20 M. I. Eremets, A. G. Gavriliuk, I. A. Trojan, D. A. Dzivenko and R. Boehler, *Nat. Mater.*, 2004, **3**, 558.
- 21 M. I. Eremets, M. Yu. Popov, I. A. Trojan, V. N. Denisov, R. Boehler and R. J. Hemley, *J. Chem. Phys.*, 2004, **120**, 10618.
- 22 M. I. Eremets, R. J. Hemley, H.-K. Mao and E. Gregoryanz, *Nature*, 2001, **411**, 170.
- 23 P. C. Samartzis, J. J.-M. Lin, T.-T. Ching, C. Chaudhuri, Y. T. Lee, S.-H. Lee and A. M. Wodtke, *J. Chem. Phys.*, 2005, **123**, 051101.
- 24 F. Cacace, G. de Petris and A. Troiani, *Science*, 2002, **295**, 480.
- 25 M. N. Glukhovtsev, H. Jiao and P. V. R. Schleyer, *Inorg. Chem.*, 1996, **35**, 7124.
- 26 S. Ajith Perera and R. J. Bartlett, *Chem. Phys. Lett.*, 1999, **314**, 381.
- 27 W. J. Lauderdale, J. F. Stanton and R. J. Bartlett, *J. Phys. Chem.*, 1992, **96**, 1173.
- 28 G. A. Olah, G. K. Surya Prakash and G. Rasul, *J. Am. Chem. Soc.*, 2001, **123**, 3308.
- 29 A. Vij, J. G. Pavlovich, W. W. Wilson, V. Vij and K. O. Christe, *Angew. Chem., Int. Ed.*, 2002, **41**, 3051.
- 30 A. Vij, W. W. Wilson, V. Vij, F. S. Tham and J. A. Sheehy, *J. Am. Chem. Soc.*, 2001, **123**, 6308.
- 31 H. Östmark, S. Wallin, T. Brinck, P. Carlqvist, R. Claridge, E. Hedlund and L. Yudina, *Chem. Phys. Lett.*, 2003, **379**, 539.
- 32 K. O. Christe, W. W. Wilson, J. A. Sheehy and J. A. Boatz, *Angew. Chem., Int. Ed.*, 1999, **38**, 2004.
- 33 R. Haiges, S. Schneider, T. Schroer and K. O. Christe, *Angew. Chem., Int. Ed.*, 2004, **43**, 4919.
- 34 M. T. Nguyen, *Coord. Chem. Rev.*, 2003, **244**, 93.
- 35 H. Huber, *Angew. Chem., Int. Ed.*, 1982, **21**, 64.
- 36 P. Saxe and H. F. Schaefer III, *J. Am. Chem. Soc.*, 1983, **105**, 1760.
- 37 T. M. Klapötke, *THEOCHEM*, 2000, **499**, 99.
- 38 M. N. Glukhovtsev and P. V. R. Schleyer, *Chem. Phys. Lett.*, 1992, **198**, 547.
- 39 M. Tobita and R. J. Bartlett, *J. Phys. Chem. A*, 2001, **105**, 4107.
- 40 B. Hirshberg and R. Benny Gerber, *Chem. Phys. Lett.*, 2012, **531**, 46.
- 41 L. J. Wang, P. Warburton and P. G. Mezey, *J. Phys. Chem. A*, 2002, **106**, 2748.
- 42 T. M. Klapötke and R. D. Harcourt, *THEOCHEM*, 2001, **541**, 237.
- 43 S. Fau and R. J. Bartlett, *J. Phys. Chem. A*, 2001, **105**, 4096.
- 44 U. N. Patil, N. R. Dhumal and S. P. Gejji, *Theor. Chem. Acc.*, 2004, **112**, 27.
- 45 M. R. Manaa, *Chem. Phys. Lett.*, 2000, **331**, 262.
- 46 S. Fau, K. J. Wilson and R. J. Bartlett, *J. Phys. Chem. A*, 2002, **106**, 4639.
- 47 L. J. Wang and M. Z. Zgierski, *Chem. Phys. Lett.*, 2003, **376**, 698.
- 48 S. J. Clark, M. D. Segall, C. J. Pickard, P. J. Hasnip, M. J. Probert, K. Refson and M. C. Payne, *Z. Kristallogr.*, 2005, **220**, 567.
- 49 *Materials Studio 7.0*, Accelrys, Inc., San Diego, CA, 2013.
- 50 J. P. Perdew, K. Burke and M. Ernzerhof, *Phys. Rev. Lett.*, 1996, **77**, 3865.
- 51 J. P. Perdew, A. Ruzsinszky, G. I. Csonka, O. A. Vydrov, G. E. Scuseria, L. A. Constantin, X. Zhou and K. Burke, *Phys. Rev. Lett.*, 2008, **100**, 136406.
- 52 A. V. Krukau, O. A. Vydrov, A. F. Izmaylov and G. E. Scuseria, *J. Chem. Phys.*, 2006, **125**, 224106.
- 53 G. Kresse and D. Joubert, *Phys. Rev. B: Condens. Matter Mater. Phys.*, 1999, **59**, 1758–1775.
- 54 P. Giannozzi, S. Baroni, N. Bonini, M. Calandra, R. Car, C. Cavazzoni, D. Ceresoli, G. L. Chiarotti, M. Cococcioni, I. Dabo, A. Dal Corso, S. Fabris, G. Fratesi, S. de Gironcoli, R. Gebauer, U. Gerstmann, C. Gougoussis, A. Kokalj, M. Lazzeri, L. Martin-Samos, N. Marzari, F. Mauri, R. Mazzarello, S. Paolini, A. Pasquarello, L. Paulatto, C. Sbraccia, S. Scandolo, G. Sclauzero, A. P. Seitsonen, A. Smogunov, P. Umari and R. M. Wentzcovitch, *J. Phys.: Condens. Matter*, 2009, **21**, 395502.
- 55 A. Tkatchenko and M. Scheffler, *Phys. Rev. Lett.*, 2009, **102**, 073005.
- 56 S. V. Bondarchuk and B. F. Minaev, *RSC Adv.*, 2015, **5**, 11558.
- 57 J. A. Alarco, A. Chou, P. C. Talbota and I. D. R. Mackinnon, *Phys. Chem. Chem. Phys.*, 2014, **16**, 24443–24456.
- 58 Virtual NanoLab 2015.1, QuantumWise A/S, www.quantumwise.com.
- 59 W. Setyawan and S. Curtarolo, *Comput. Mater. Sci.*, 2010, **49**, 299.
- 60 G. M. Dongho Nguimdoa and D. P. Joubert, *Eur. Phys. J. B*, 2015, **88**, 113.

- 61 L. Mitas and R. M. Martin, *Phys. Rev. Lett.*, 1994, **72**, 2438.
- 62 S. V. Bondarchuk and B. F. Minaev, submitted to journal.
- 63 M. Sheik-Bahae. Nonlinear Optics Basics. Kramers–Kronig Relations in Nonlinear Optics, in *Encyclopedia of Modern Optics*, ed. R. D. Guenther, Academic Press, Amsterdam, 2005, pp. 234–239.
- 64 C. J. Pickard and F. Mauri, *Phys. Rev. B: Condens. Matter Mater. Phys.*, 2001, **63**, 245101.
- 65 S. L. Veinberg, K. E. Johnston, M. J. Jaroszewicz, B. M. Kispal, C. R. Mireault, T. Kobayashi, M. Pruski and R. W. Schurko, *Phys. Chem. Chem. Phys.*, 2016, **18**, 17713–17730.
- 66 E. Dib, T. Mineva and B. Alonso, *Annu. Rep. NMR Spectrosc.*, 2016, **87**, 175.
- 67 M. Dračinský, M. Šála, B. Klepetářová, J. Šebera, J. Fukal, V. Holečková, Y. Tanaka, R. Nencka and V. Sychrovský, *J. Phys. Chem. B*, 2016, **120**, 915–925.
- 68 F. Mouhat and F.-X. Coudert, *Phys. Rev. B: Condens. Matter Mater. Phys.*, 2014, **90**, 224104.
- 69 J. F. Nye, *Physical properties of crystals*, Oxford University Press Inc., Oxford, 1985.
- 70 C. A. Klein and G. F. Cardinale, *Diamond Relat. Mater.*, 1993, **2**, 918–923.
- 71 A. Hu, F. Zhang and T. Woo, *Phys. Rev. B: Condens. Matter Mater. Phys.*, 2010, **82**, 125410.
- 72 Y. Li, J. Hao, H. Liu, S. Lu and J. S. Tse, *Phys. Rev. Lett.*, 2015, **115**, 105502.
- 73 M. J. Kamlet and S. J. Jacobs, *J. Chem. Phys.*, 1968, **48**, 23.
- 74 S. Gupta, S. K. Sengupta and H. J. Singh, *Propellants, Explos., Pyrotech.*, 2016, **41**, 645.
- 75 D. Srinivas and V. D. Ghule, *RSC Adv.*, 2016, **6**, 7712.
- 76 A. A. Gidaspov, V. A. Zalomenkov, V. V. Bakharev, V. E. Parfenov, E. V. Yurtaev, M. I. Struchkova, N. V. Palysaeva, K. Y. Suponitsky, D. B. Lempertd and A. B. Sheremetev, *RSC Adv.*, 2016, **6**, 34921.
- 77 N. N. Karaush, S. V. Bondarchuk, G. V. Baryshnikov, V. A. Minaeva, W.-H. Sun and B. F. Minaev, *RSC Adv.*, 2016, **6**, 49505.